The Effect of Downstream Plasma Treatments on Graphene Surfaces

Nikolaos Peltekis, Shishir Kumar, Niall McEvoy, Kangho Lee, Anne Weidlich, Georg S. Duesberg

PII: S0008-6223(11)00699-3
DOI: 10.1016/j.carbon.2011.08.052
Reference: CARBON 6791

To appear in: *Carbon*

Received Date: 8 June 2011
Accepted Date: 26 August 2011

Please cite this article as: Peltekis, N., Kumar, S., McEvoy, N., Lee, K., Weidlich, A., Duesberg, G.S., The Effect of Downstream Plasma Treatments on Graphene Surfaces, *Carbon* (2011), doi: 10.1016/j.carbon.2011.08.052

The Effect of Downstream Plasma Treatments on Graphene Surfaces

Nikolaos Peltekis[1], *Shishir Kumar*[1], *Niall McEvoy*[1], *Kangho Lee*[1,2], *Anne Weidlich*[1], *Georg S. Duesberg*[1*]

[1]Centre for Research on Adaptive Nanostructures and Nanodevices (CRANN) and

School of Chemistry, Trinity College Dublin, College Green, Dublin 2, Ireland

[2]School of Electrical Engineering, Korea University, Seoul, 136-713, South Korea

Abstract: This paper reports on the effects of growth, transfer and annealing procedures on graphene grown by chemical vapour deposition. A combination of Raman spectroscopy, electrical measurements, atomic force microscopy, and x-ray photoemission spectroscopy allowed for the study of inherent characteristics and electronic structure of graphene films. Contributions from contaminants and surface inhomogeneities such as ripples were also examined. A new cleaning and reconstruction process for graphene, based on plasma treatments and annealing is presented, opening a new pathway for control over the surface chemistry of graphene films. The method has been successfully used on contacted graphene samples, demonstrating its potential for in-situ cleaning, passivation and interface engineering of graphene devices.

[*] Corresponding author. Tel/Fax: +353(1) 8963035. E-mail address: duesberg@tcd.ie (G.S. Duesberg)

1. Introduction

The unique electronic properties of graphene make it of high interest for electronic devices. The two-dimensional single layer of sp^2-hybridized carbon atoms has charge carriers that exhibit giant intrinsic mobility, have zero effective mass and can travel for micrometers without scattering at room temperature[1]. In combination with a record thermal conductivity at room temperature (~5000$Wm^{-1}K^{-1}$)[2], the possibility of structuring and tuning its properties[3] make it an ideal candidate for use in future devices in electronics and energy harvesting such as conducting electrodes[4-7], switches[8-12], spintronics[13-15] and sensors[16-19]. The quality and surface chemistry of graphene is crucial for these applications, as contamination, impurities, morphology and defects can substantially affect its electronic properties and performance in these devices[20-23]. To date, most studies have focused on graphene produced by mechanical exfoliation and thermal decomposition of SiC. However, the processability and scalability of these processes is limited[1, 24]. The emergence of chemical vapour deposition (CVD) as a growth method has yielded macroscale samples, but these are of varying quality. CVD growth of graphene is a promising industry adapted method. However, post growth processing steps such as transferring and structuring are often aggressive and can cause substrate-induced structural distortion[21], adsorbates[25], local charge disorder[20], atomic structure at the edges[22, 26], atomic scale defects[23] and effects of trapped oxide charges[27]. These are some of the common factors that one comes across when processing graphene and they can substantially deteriorate its performance, thus it is essential to control the surface chemistry of graphene layers to allow for passivation, controlled functionalization and reliable electrical response. Controlling the surface chemistry of a monolayer during processing is a difficult task, especially when working in ambient conditions. For CVD grown films it has been reported that polymer residue

among other absorbed contaminants dominate graphene substrates after structuring, thus extra cleaning steps are required[28, 29]. A few reports propose annealing in vacuum or an ambient atmosphere of forming gas[28-30] which appears, in some cases, to improve graphene's conductivity[29]. Plasma treatments have previously been used to modify the surface properties of thick graphene based films[31]. However, when dealing with CVD grown graphene films the experimental parameters have to be carefully controlled to minimise surface damage.

In this work we present a comprehensive study on large area CVD grown graphene films using Raman, x-ray photoemission spectroscopy (XPS) and microscopy (atomic force and scanning electron microscopy AFM/SEM). We study the effects of growth, transfer and annealing procedures on the electronic properties of graphene. Furthermore, a new cleaning and reconstructing process of graphene is presented based on plasma cleaning and annealing. The plasma treatment was used as a post-processing step on contacted graphene layers, improving their electrical performance, a crucial ingredient for the applicability of graphene. With extensive analysis based on high resolution C1s spectra, the study further establishes XPS as a powerful tool for graphene characterization, capable of determining metallicity, defect density and contamination on graphene samples. The microscopic examinations reveal that more detailed features become apparent after our cleaning procedures. Thus careful plasma treatments can be used to manipulate the surface chemistry of graphene layers.

2. Experimental

2.1 Sample preparation

CVD growth and transfer process of graphene: Graphene has been grown on copper following the method presented by Li et al[32]. After CVD growth in a Gero tube furnace with methane at

950 °C a thin film of PMMA was spin-coated on top of graphene grown on Cu foils. Thermal tape was applied on top of the PMMA layer for a rigid support and then the underlying copper was etched using $FeCl_3$ solution (1 M). The resulting films were washed with deionised water and placed on top of suitable substrates with the graphene side in contact with the surface. Uniform pressure and heat (150 °C) was applied on the film, this melted the PMMA and made it conform to substrate topology. The heat also allowed the thermal tape to dissociate, after which it was removed. The PMMA layer on the substrate was dissolved with acetone, leaving behind graphene adhered to the substrate surface. The plasma was generated by a commercial microwave radical generator (R^3T TWR 2000-GEN, 400V) in DC mode with a power output of 1000 W. Samples were positioned ~50 cm from the plasma source. In this position the plasma generated ions were energetically relaxed upon arrival at the sample and thus the plasma could be considered remote, minimising surface damage.

2.2 Sample Characterization

AFM imaging was performed with an Asylum Research MFP-3D system in tapping mode using Si cantilevers. SEM images were acquired on a Zeiss Ultra Plus with InLens detector. A Horiba Jobin Yvon LabRAM with a 633 nm laser excitation line was employed for Raman spectroscopy. The XPS measurements were taken by an Omicron ESCA system installed with an EA 125 Analyzer and XM1000MK II monochromised x-ray source. This Al Kα x-ray source gives a spot of 2 mm in diameter. The analyzer (5 channel detector) was operated with the largest entrance and exit slits and with pass energy Ep = 20 eV for the C1s spectra. The total combined instrumental resolution instrument was ~0.68 eV for the C1s spectra. Electrical characterization was performed on a Suess needle prober with a Keithley Instruments model 2602 sourcemeter at room temperature in ambient conditions.

3. Results and Discussion

3.1 Pristine graphene

Raman and XPS spectra of as grown graphene on Cu are presented in Fig.1. The Raman spectrum shows distinct G and 2D peaks associated with long range ordered graphitic sp^2 carbon. The intensity ratio of the 2D to G (1584 cm^{-1}) peaks is, $I_{2D/G} = 2.54$ and the 2D peak (at 2663 cm^{-1}) can be well fitted with one Lorentzian peak with a width of 37.2 cm^{-1}. These factors indicate the presence of monolayer graphene[33, 34]. This monolayer signal was consistent over the entire sample area and is comparable with literature spectra for graphene grown on Cu[32]. This is significantly different to graphene grown on Ni substrates which typically consists of domains of few layer (FLG) and monolayer graphene [35, 36]. The fact that the D peak is marginal and the D' (which occurs via an intra-valley double-resonance process in the presence of defects[37]) is absent, indicates a graphene layer of high crystallinity and low defect density. The XPS spectrum (Fig. 1b) has a well pronounced asymmetry on the higher binding energy side typical of polyaromatic carbons[38-41]. This implies graphitic structure and conducting films as opposed to non-conducting aliphatic or sp^3 based carbon materials which exhibit symmetric spectra[38]. The spectrum has been fitted accordingly with several peaks that describe different chemical carbon functionalities by taking into account the combined instrumental resolution of the XPS system. The main peak at 284.2 eV has been fitted with a Doniach-Sunjic function[42] which best reproduces the asymmetry on the higher binding energy side. This is an intrinsic property of the system based on the many electron interaction as described from Mahan[43] and Nozieres & DeDominicis[41]. The asymmetry can be measured by the singularity asymmetry factor α, which relates to the density of states of the valence band and the rearrangement of the

Fermi-edge electron sea upon the creation of a core hole. It can be used as a measure of the screening of the core hole which depends on the level of delocalization of the valence states. It thus gives an indication of the in-plane order and the level of defects and imperfections on the graphitic net. The delocalization is of great importance for the electronic properties and strongly relates to the electrical conductivity of graphene. The peak has an asymmetry factor α = 0.07, smaller than that of graphite which has been reported as 0.15[38]. Highly disordered graphitic structures, such as pyrolytic carbon, for example have higher asymmetry factors (α=0.19[38]). This is due to the larger surface area of edges resulting in higher surface contamination. Slight differential charging is created on disordered sheets (no differential charging on graphite is observed as it is conductive), thus disorder and defects create excitonic states and excitonic screening[38]. The smaller singularity asymmetry factor indicates a graphitic net with higher delocalization of electrons. There is a second peak at 284.8 eV which accounts for sp^3 hybridized carbon bonds due to amorphous aliphatic carbon contaminants and defects. The relatively small height of this peak compared to the graphitic peak indicates marginal traces of other carbon functionalities and an intact graphitic lattice.

3.2 Transferred graphene

A typical AFM image, Raman and XPS spectra of graphene transferred onto SiO_2 are depicted in Figure 2. The AFM image (Fig.2a) shows a substantial amount of contamination on the surface, most likely due to polymer residue, resulting in a root mean square (RMS) roughness value of 11 nm. Furthermore, looking in detail at the step height of the graphene layer to the substrate gives a value of 1.2 nm which is higher than that previously reported for mechanically exfoliated monolayer graphene (~0.7 nm[44]). However, this value is consistent with previously reported values for monolayer regions of transferred CVD graphene[36]. This suggests that a

thin layer, most likely polymer residue, remains on top of the graphene. Looking at the Raman spectrum as depicted in Figure 2b, there are still pronounced G and 2D bands, but a distinct D band is also observed. The enhancement of the D band could be a result of defects created during the transfer process. The intensity ratio 2D to G peaks is now $I_{2D/G} = 1.27$. The 2D peak is downshifted to 2646 cm^{-1}, whereas the width is relatively unchanged (37.7 cm^{-1}). Encasement of defects could be responsible for the intensity reduction, whereas the shift could be due to induced charge from dopants[45] (contamination), extra layers[33, 34] or induced strain[46] as the 2D peak is sensitive to these factors. The situation is further clarified in the XPS spectrum of the same sample shown in Fig.2c. The C1s core level spectrum, fitted in a similar fashion as before, reveals a substantial signal of sp^3 hybridization[47-49] along with other carbon functionalities, such as C-N[50, 51], C-OH[52, 53], C=O[47, 52, 53], COOH/R[47, 52, 53], CF-C/C-CF_n[54-56] as previously reported in the literature. The asymmetry factor α on the graphitic peak is increased to 0.1, considerably higher than the as grown sample. These results show that the transfer process induces a substantial amount of impurities and different functionalities which are known to alter and in most cases to substantially downgrade graphene's properties[25, 28].

In an attempt to clean the graphene surface and remove the contaminants we first investigated annealing procedures as have been reported previously in the literature[28-30]. Two different cases formed the focus of this investigation. In the first case a few layer graphene sample that was grown on a Ni substrate (growth details Kumar et al [57]) was transferred onto a SiO_2 substrate without the use of polymer support. The sample underwent annealing in forming gas (Ar:H_2, 9:1) for 10 hours at 900 ˚C. In Figure 3a C1s core level XPS spectra from this sample before and after the annealing step are shown. The full width half maximum (FWHM) of the peak is reduced from 1.32 eV to 0.8 eV after annealing, which is close to instrumental

resolution (0.68 eV). This indicates that the annealing led to the removal of substantial amounts of contaminants. In the second case the same experiment was conducted using monolayer graphene which was transferred using polymer support. The C1s peak of the two different samples annealed in the same fashion at 650 ˚C and 900 ˚C are shown in Figure 3b. In the best case (at 900 ˚C) the FWHM was 1.4 eV, which suggests that annealing does not remove polymer residues, whereas this is feasible for low molecular weight adsorbents as shown in the first case.

3.3 Plasma treatment of transferred graphene

The use of plasma treatment as a cleaning step has been investigated. Few layer graphene, transferred as before on SiO_2, was treated with oxygen plasma for two minutes. This was carried out in a chamber under a constant pressure of 1 torr and with an oxygen flow rate of 100 sccm controlled by a mass flow controller (MFC). The sample was then annealed for 10 hours in forming gas at 900 ˚C.

Figure 4a shows C1s XPS spectra of the sample before and after the annealing. The non-annealed sample has C1s peak shifted to higher energies, with a FWHM of 1.2 eV. The peak also shows asymmetry on the higher energy side. An extra small peak appears in the spectrum at 286.2 eV which is due to epoxide formation on the graphitic net. The asymmetry indicates the presence of graphene. The shift to higher binding energy and the FWHM suggest the creation of defects on the graphitic net. After the annealing the spectrum looks sharper and still displays asymmetry on the higher binding energy side. The peak has shifted to lower binding energy and the epoxide peak has disappeared. The spectrum has a FWHM of 0.68 eV as extrapolated from the analytical fitting shown in Fig 4b. This is exactly the same as the instrumental resolution and indicates a perfectly clean graphitic signal. There are no traces of any kind of carbon functional

groups. The lower binding energy at 284.19 eV is due to better screening and extensive delocalization. This gives a strong indication that curing of defects on the graphitic net occurs. The singularity asymmetry factor α is 0.12. The singularity asymmetry factor α could be an indication of thickness (layers) in a clean graphitic net as it increases with increasing number of layers; 0.07 for monolayer, 0.12 for a few layers and 0.14[38] for graphite. In Figure 4c Raman spectra before and after the annealing are shown. There is a reduction in the D peak after annealing that further confirms curing of the graphitic net.

A slightly different approach was implemented for the treatment of monolayer graphene. In this case a more delicate approach was adopted to minimise damage to the graphene. Four continuous cycles of 5 min oxygen plasma treatment with a 60 sccm flow rate at 180 ˚C were followed by 10 min of hydrogen plasma treatment with a 50 sccm flow rate at 270 ˚C. The temperature was intentionally kept below 300 ˚C in order to make this method suitable for structured graphene samples with metal contacts that are sensitive to high temperatures. In Figure 5a an AFM image of the treated sample is shown. The surface looks much cleaner and has a much smaller RMS roughness value of 2.9 nm compared to the untreated case. The step height from substrate to graphene is 0.42 nm, which is close to the theoretical monolayer value (0.34 nm) and is much smaller than what has been published previously for monolayer graphene[44]. The higher magnification image in Figure 5b shows distinguishable ripples and wrinkles on graphene which weren't observable before the treatment. It's not clear if the wrinkles were covered underneath an overlayer of contaminants and only became visible upon their removal, or if they were created after the treatment. Wrinkle formation has been reported before and was related to the thermal expansion coefficient difference between Cu and graphene[32] Further, strain has also been reported to create wrinkles[58] which are possibly induced during the

transfer process or even due to the shrinkage of the polymer overlayer. As an alternative explanation functionalization that occurs during the plasma treatment could also cause shrinkage or bending of areas on the sample[59, 60].

In Figure 5c a large area (~20x20 μm) SEM image of plasma treated graphene is presented. It proves that this method cleans large area graphene films leaving them intact. It is apparent that distinct features become visible which were not resolved prior to cleaning, similar to the observation in the AFM image. The C1s core level spectrum of the sample is shown in Figure 6a. The spectrum comes with an asymmetry on the higher binding energy side of the peak which is located at 284.28 eV. The higher singularity asymmetry factor α of 0.08 and the slightly higher binding energy, compared to the spectrum of as grown graphene on Cu shown earlier, indicate a slightly defective graphitic net. Importantly, a second fitted peak at 284.8 eV, which accounts for amorphous carbon content and sp^3 defects, has been substantially diminished, confirming that contributions from polymer residue contaminant have been significantly reduced. Some traces of oxygen bonded carbon groups remain after the treatment. The remaining peak at 284.8 eV related to sp^3 bonds in the graphitic net, may be explained by hydrogen incorporation during the hydrogen plasma step[37]. Raman spectra of the three different steps are compared in Figure 6b. The Raman spectrum after the cleaning shows an enhanced D peak which is indicative of defective graphitic structure and is in agreement with the XPS observations. The G and 2D appear broadened and the intensity ratio is $I_{2D/G}$= 0.71. The G peak is upshifted and set at 1600 cm^{-1} with a larger width as satellite peaks appear on both sides from the main peak. The shift cannot be attributed to doping from contaminants since their concentration has reduced after treatment as shown in the XPS spectrum. A similar Raman spectrum has previously been reported for hydrogen functionalized graphene on a SiO_2 substrate

[37]. In this study the shift was only noticeable on graphene laying on a substrate and not on suspended graphene. In the first case functionalization occurs only on the top side of the graphene. This could cause bending of the graphitic net and splitting of the G band as is the case for single wall carbon nanotubes.[61] This could also account for the shift observed. The 2D band is broadened and centred at 2662 cm^{-1} and again is indicative of a defective and curved graphitic net signal.

3.4 In-situ plasma treatment of contacted graphene

To show the suitability of this cleaning method for structured samples, contacted graphene ribbons, which were fabricated as described elsewhere[42] were measured electrically before and after the plasma cleaning treatment. Graphene ribbons exhibited linear source-drain current versus bias voltages (I_{ds}-V_{ds}) characteristics and the conductivity increased approximately 1.5-6 times after the plasma treatment process (Fig. 7(a)). Typical ambipolar characteristics for graphene, with a higher hole conduction and hysteresis were observed in both cases. The field-effect mobility was calculated using the conventional method as defined by the following equation;

$$\mu = \frac{1}{C_{ox}} \frac{L}{W} \frac{\partial I_{ds}}{\partial V_{gs}} \frac{1}{V_{ds}}$$

where L is the length of graphene ribbons, W the width, C_{ox} the capacitance of the dielectric.

The dependence of the source-drain current on gate voltage is shown in Fig. 7(b). The graphene ribbons have electron and hole field-effect mobilities of 11.2 and 31.9 cm^2/Vs respectively prior to treatment and 44.8 and 143.6 cm^2/Vs respectively after treatment, which is

an increase of a factor 4.. This value is less than the best CVD graphene values previously reported by Li et al.[32]. However, their values were obtained on full films rather than ribbons, in a dual gated structure on Al_2O_3 substrates meaning that their effective field was much larger than ours. We emphasize that these are preliminary results and show the potential of this method when it is applied to contacted graphene. Whilst the focus of this paper is the cleaning of transferred graphene samples it is expected that such plasma treatments could be modified in order to introduce controlled levels of defects and functionalities into contacted samples, thus giving tuneable device properties[62].

4. Summary

A comprehensive study involving AFM, Raman and XPS spectroscopies shows that graphene's quality is substantially affected during the transfer and structuring processes. AFM reveals an overlayer content which is believed to be polymer residue as characterized by C1s core level XPS. Also XPS and Raman indicate the creation of defects during the transfer process as seen in the enhancement of the D band in Raman spectra and the rise of sp^3 peak in the C1s XPS spectrum. Annealing with forming gas helps to remove small molecules adsorbents but cannot remove polymer residue as proven by C1s core level XPS analysis. A novel cleaning method based on remote plasma treatment in combination with annealing at 900 ˚C with forming gas can yield perfectly clean and less defective few layer graphene as demonstrated with XPS and Raman analysis. A more delicate plasma treatment implemented on graphene devices was effective in removing most of the residual polymer with little effect on the graphene. I-V measurements conducted with this cleaning method show higher conductivity and enhanced mobilities up to 200 cm^2/Vs.

References

[1] Geim AK. Graphene: Status and Prospects. Science. 2009 June 19, 2009;324(5934):1530-4.

[2] Balandin AA, Ghosh S, Bao W, Calizo I, Teweldebrhan D, Miao F, et al. Superior Thermal Conductivity of Single-Layer Graphene. Nano Letters. 2008;8(3):902-7.

[3] Melinda YH, Barbaros O, Yuanbo Z, Philip K. Energy Band-Gap Engineering of Graphene Nanoribbons. Physical Review Letters. 2007;98(20):206805.

[4] Cai WW, Zhu YW, Li XS, Piner RD, Ruoff RS. Large area few-layer graphene/graphite films as transparent thin conducting electrodes. Applied Physics Letters. 2009 Sep;95(12).

[5] Wang X, Zhi L, Mullen K. Transparent, Conductive Graphene Electrodes for Dye-Sensitized Solar Cells. Nano Letters. 2008;8(1):323-7.

[6] De S, King PJ, Lotya M, O'Neill A, Doherty EM, Hernandez Y, et al. Flexible, Transparent, Conducting Films of Randomly Stacked Graphene from Surfactant-Stabilized, Oxide-Free Graphene Dispersions. Small. 2010;6(3):458-64.

[7] Eda G, Fanchini G, Chhowalla M. Large-area ultrathin films of reduced graphene oxide as a transparent and flexible electronic material. Nature Nanotechnology. 2008 May;3(5):270-4.

[8] Lemme MC, Echtermeyer TJ, Baus M, Kurz H. A graphene field-effect device. IEEE Electron Device Lett. 2007 Apr;28(4):282-4.

[9] Meric I, Han MY, Young AF, Ozyilmaz B, Kim P, Shepard KL. Current saturation in zero-bandgap, top-gated graphene field-effect transistors. Nat Nano. 2008;3(11):654-9.

[10] Stampfer C, Schurtenberger E, Molitor F, Guttinger J, Ihn T, Ensslin K. Tunable graphene single electron transistor. Nano Letters. 2008 Aug;8(8):2378-83.

[11] Zhang Q, Fang T, Xing HL, Seabaugh A, Jena D. Graphene Nanoribbon Tunnel Transistors. IEEE Electron Device Lett. 2008 Dec;29(12):1344-6.

[12] Zhang YB, Tang TT, Girit C, Hao Z, Martin MC, Zettl A, et al. Direct observation of a widely tunable bandgap in bilayer graphene. Nature. 2009 Jun;459(7248):820-3.

[13] Maassen J, Ji W, Guo H. Graphene Spintronics: The Role of Ferromagnetic Electrodes. Nano Letters. 2011 Jan;11(1):151-5.

[14] Son YW, Cohen ML, Louie SG. Half-metallic graphene nanoribbons. Nature. 2006 Nov;444(7117):347-9.

[15] Tombros N, Jozsa C, Popinciuc M, Jonkman HT, van Wees BJ. Electronic spin transport and spin precession in single graphene layers at room temperature. Nature. 2007 Aug;448(7153):571-U4.

[16] Ang PK, Chen W, Wee ATS, Loh KP. Solution-Gated Epitaxial Graphene as pH Sensor. Journal of the American Chemical Society. 2008 Nov;130(44):14392-+.

[17] Fowler JD, Allen MJ, Tung VC, Yang Y, Kaner RB, Weiller BH. Practical Chemical Sensors from Chemically Derived Graphene. ACS Nano. 2009 Feb;3(2):301-6.

[18] Huang B, Li ZY, Liu ZR, Zhou G, Hao SG, Wu J, et al. Adsorption of gas molecules on graphene nanoribbons and its implication for nanoscale molecule sensor. Journal of Physical Chemistry C. 2008 Sep;112(35):13442-6.

[19] Keeley GP, O'Neill A, McEvoy N, Peltekis N, Coleman JN, Duesberg GS. Electrochemical ascorbic acid sensor based on DMF-exfoliated graphene. Journal of Materials Chemistry. 2010;20(36):7864-9.

[20] Hwang EH, Adam S, Das Sarma S. Transport in chemically doped graphene in the presence of adsorbed molecules. Physical Review B. 2007;76(19):195421.

[21] Morozov SV, Novoselov KS, Katsnelson MI, Schedin F, Ponomarenko LA, Jiang D, et al. Strong Suppression of Weak Localization in Graphene. Physical Review Letters. 2006;97(1):016801.

[22] Niimi Y, Matsui T, Kambara H, Tagami K, Tsukada M, Fukuyama H. Scanning tunneling microscopy and spectroscopy of the electronic local density of states of graphite surfaces near monoatomic step edges. Physical Review B. 2006;73(8):085421.

[23] Wehling TO, Balatsky AV, Katsnelson MI, Lichtenstein AI, Scharnberg K, Wiesendanger R. Local electronic signatures of impurity states in graphene. Physical Review B. 2007;75(12):125425.

[24] Berger C, Song Z, Li T, Li X, Ogbazghi AY, Feng R, et al. Ultrathin Epitaxial Graphite: 2D Electron Gas Properties and a Route toward Graphene-based Nanoelectronics. The Journal of Physical Chemistry B. 2004;108(52):19912-6.

[25] Schedin F, Geim AK, Morozov SV, Hill EW, Blake P, Katsnelson MI, et al. Detection of individual gas molecules adsorbed on graphene. Nat Mater. 2007;6(9):652-5.

[26] Nakada K, Fujita M, Dresselhaus G, Dresselhaus MS. Edge state in graphene ribbons: Nanometer size effect and edge shape dependence. Physical Review B. 1996;54(24):17954.

[27] Jayaraman R, Sodini CG. A 1/f noise technique to extract the oxide trap density near the conduction band edge of silicon. Electron Devices, IEEE Transactions on. 1989;36(9):1773-82.

[28] Ishigami M, Chen JH, Cullen WG, Fuhrer MS, Williams ED. Atomic Structure of Graphene on SiO2. Nano Letters. 2007;7(6):1643-8.

[29] Moser J, Barreiro A, Bachtold A. Current-induced cleaning of graphene. Applied Physics Letters. 2007;91(16):163513-3.

[30] Stolyarova E, Rim KT, Ryu S, Maultzsch J, Kim P, Brus LE, et al. High-resolution scanning tunneling microscopy imaging of mesoscopic graphene sheets on an insulating surface. Proceedings of the National Academy of Sciences. 2007 May 29, 2007;104(22):9209-12.

[31] Xie X, Qu L, Zhou C, Li Y, Zhu J, Bai H, et al. An Asymmetrically Surface-Modified Graphene Film Electrochemical Actuator. ACS Nano. 2010;4(10):6050-4.

[32] Li X, Cai W, An J, Kim S, Nah J, Yang D, et al. Large-Area Synthesis of High-Quality and Uniform Graphene Films on Copper Foils. Science. 2009 June 5, 2009;324(5932):1312-4.

[33] Ferrari AC, Meyer JC, Scardaci V, Casiraghi C, Lazzeri M, Mauri F, et al. Raman Spectrum of Graphene and Graphene Layers. Physical Review Letters. 2006;97(18):187401.

[34] Malard LM, Nilsson J, Elias DC, Brant JC, Plentz F, Alves ES, et al. Probing the electronic structure of bilayer graphene by Raman scattering. Physical Review B. 2007;76(20):201401.

[35] Chae SJ, Gunes F, Kim KK, Kim ES, Han GH, Kim SM, et al. Synthesis of Large-Area Graphene Layers on Poly-Nickel Substrate by Chemical Vapor Deposition: Wrinkle Formation. Advanced Materials. 2009 Jun;21(22):2328-+.

[36] Reina A, Jia X, Ho J, Nezich D, Son H, Bulovic V, et al. Large Area, Few-Layer Graphene Films on Arbitrary Substrates by Chemical Vapor Deposition. Nano Letters. 2009;9(1):30-5.

[37] Elias DC, Nair RR, Mohiuddin TMG, Morozov SV, Blake P, Halsall MP, et al. Control of Graphene's Properties by Reversible Hydrogenation: Evidence for Graphane. Science. 2009 Jan;323(5914):610-3.

[38] Cheung TTP. X-ray photoemission of carbon: Lineshape analysis and application to studies of coals. Journal of Applied Physics. 1982;53(10):6857-62.

[39] Darmstadt H, Roy C. Surface spectroscopic study of basic sites on carbon blacks. Carbon. 2003;41(13):2662-5.

[40] Dekanski A, Stevanovic J, Stevanovic R, Nikolic BZ, Jovanovic VM. Glassy carbon electrodes: I. Characterization and electrochemical activation. Carbon. 2001;39(8):1195-205.

[41] van Attekum PMTM, Wertheim GK. Excitonic Effects in Core-Hole Screening. Physical Review Letters. 1979;43(25):1896.

[42] Doniach S, Sunjic M. Many-electron singularity in X-ray photoemission and X-ray line spectra from metals. Journal of Physics C: Solid State Physics. 1970;3(2):285.

[43] Mahan GD. Excitons in Metals: Infinite Hole Mass. Physical Review. 1967;163(3):612.

[44] Gupta A, Chen G, Joshi P, Tadigadapa S, Eklund. Raman Scattering from High-Frequency Phonons in Supported n-Graphene Layer Films. Nano Letters. 2006;6(12):2667-73.

[45] Das A, Pisana S, Chakraborty B, Piscanec S, Saha SK, Waghmare UV, et al. Monitoring dopants by Raman scattering in an electrochemically top-gated graphene transistor. Nat Nano. 2008;3(4):210-5.

[46] Mohiuddin TMG, Lombardo A, Nair RR, Bonetti A, Savini G, Jalil R, et al. Uniaxial strain in graphene by Raman spectroscopy: G peak splitting, Grüneisen parameters, and sample orientation. Physical Review B. 2009;79(20):205433.

[47] Desimoni E, Casella GI, Morone A, Salvi AM. XPS determination of oxygen-containing functional groups on carbon-fibre surfaces and the cleaning of these surfaces. Surface and Interface Analysis. 1990;15(10):627-34.

[48] Javier D, Paolicelli G, Ferrer S, Comin F. Separation of the sp3 and sp2 components in the C1s photoemission spectra of amorphous carbon films. Physical Review B. 1996;54(11):8064.

[49] Lascovich JC, Giorgi R, Scaglione S. Evaluation of the sp2/sp3 ratio in amorphous carbon structure by XPS and XAES. Applied Surface Science. 1991;47(1):17-21.

[50] Snis A, Matar SF. Electronic density of states, 1s core-level shifts, and core ionization energies of graphite, diamond, C_3N_4 phases, and graphitic $C_{11}N_4$. Physical Review B. 1999;60(15):10855.

[51] Xie Y, Sherwood PMA. X-Ray Photoelectron-Spectroscopic Studies of Carbon Fiber Surfaces. Part IX: The Effect of Microwave Plasma Treatment on Carbon Fiber Surfaces. Applied Spectroscopy. 1989;43:1153-8.

[52] Ilangovan G, Chandrasekara Pillai K. Electrochemical and XPS Characterization of Glassy Carbon Electrode Surface Effects on the Preparation of a Monomeric Molybdate(VI)-Modified Electrode. Langmuir. 1997;13(3):566-75.

[53] Pantea D, Darmstadt H, Kaliaguine S, Sümmchen L, Roy C. Electrical conductivity of thermal carbon blacks: Influence of surface chemistry. Carbon. 2001;39(8):1147-58.

[54] Carlo SR, Wagner AJ, Fairbrother DH. Iron Metalization of Fluorinated Organic Films: A Combined X-ray Photoelectron Spectroscopy and Atomic Force Microscopy Study. The Journal of Physical Chemistry B. 2000;104(28):6633-41.

[55] Limb SJ, Labelle CB, Gleason KK, Edell DJ, Gleason EF. Growth of fluorocarbon polymer thin films with high CF_2 fractions and low dangling bond concentrations by thermal chemical vapor deposition. Applied Physics Letters. 1996;68(20):2810-2.

[56] Unger E, Liebau M, Duesberg GS, Graham AP, Kreupl F, Seidel R, et al. Fluorination of carbon nanotubes with xenon difluoride. Chemical Physics Letters. 2004;399(1-3):280-3.

[57] Kumar S, McEvoy N, Lutz T, Keeley GP, Nicolosi V, Murray CP, et al. Gas phase controlled deposition of high quality large-area graphene films. Chemical Communications.46(9):1422-4.

[58] Ismach A, Druzgalski C, Penwell S, Schwartzberg A, Zheng M, Javey A, et al. Direct Chemical Vapor Deposition of Graphene on Dielectric Surfaces. Nano Letters. 2010;10(5):1542-8.

[59] Schniepp HC, Kudin KN, Li J-L, Prud'homme RK, Car R, Saville DA, et al. Bending Properties of Single Functionalized Graphene Sheets Probed by Atomic Force Microscopy. ACS Nano. 2008;2(12):2577-84.

[60] Zhiping X, Kun X. Engineering graphene by oxidation: a first-principles study. Nanotechnology. 2010;21(4):045704.

[61] Dresselhaus MS, Dresselhaus G, Saito R, Jorio A. Raman spectroscopy of carbon nanotubes. Physics Reports. 2005;409(2):47-99.

[62] Coleman VA, Knut R, Karis O, Grennberg H, Jansson U, Quinlan R, et al. Defect formation in graphene nanosheets by acid treatment: an x-ray absorption spectroscopy and density functional theory study. J Phys D-Appl Phys. 2008 Mar;41(6).

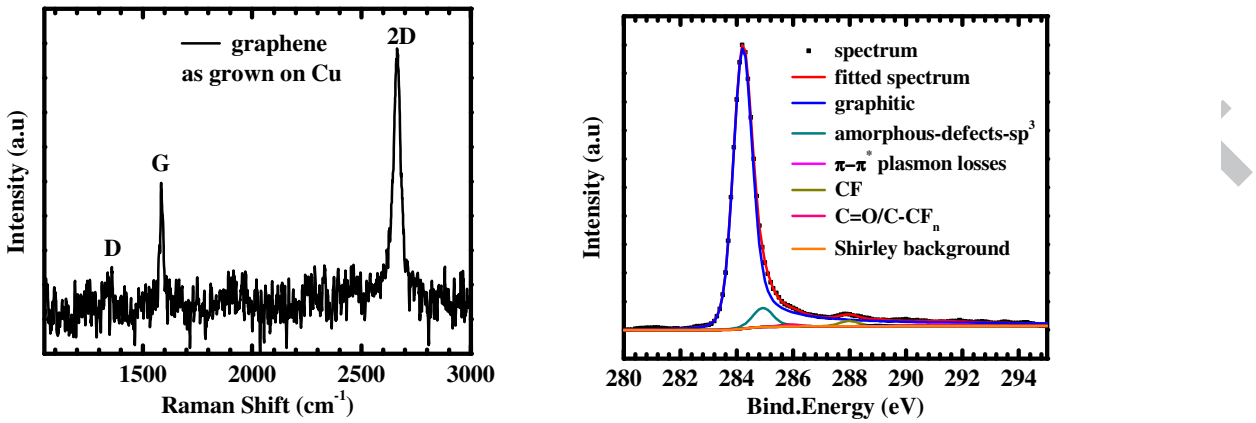

Figure 1 Raman and XPS spectra of as grown graphene on Cu a) The Raman spectrum shows a distinct 2D peak associated with long range graphitic order. The 2D peak (at 2663 cm^{-1}) can be fitted with a single Lorentzian peak with a width of 37.2 cm^{-1}, indicative of monolayer graphene[33, 34]. The fact that the D peak is marginal and D' absent indicates ahighly crystalline graphene layer with minimal contributions from defects b) C1s core level XPS spectrum fitted accordingly shows a relatively clean and highly crystalline carbon signal. The asymmetry on the higher binding energy side implies graphitic structure and metallic conductivity. This can be measured by the singularity asymmetry factor, α, which is related to the delocalization of the valence states. The peak has an asymmetry factor α = 0.07, smaller than that of graphite which has been reported as 0.15[38] . The smaller singularity asymmetry factor indicates a graphitic net with higher delocalization of electrons[38].

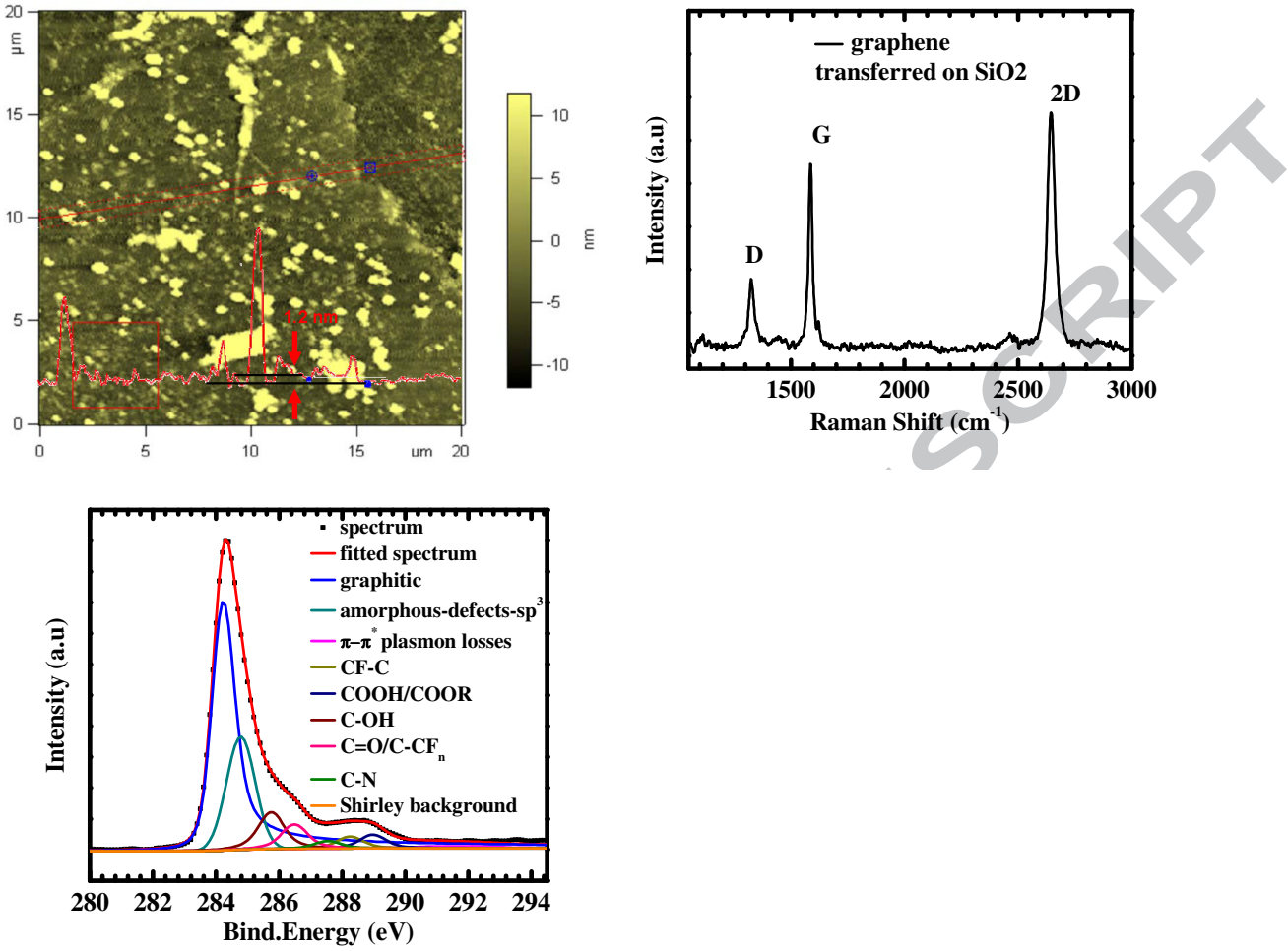

Figure 2 AFM, Raman and XPS of graphene transferred onto SiO_2. a) AFM image shows a substantial amount of contamination on the surface, (most likely due to polymer residue) giving a root mean square (RMS) roughness value of 11 nm and a step height from the graphene layer to the substrate of 1.2 nm. b) A distinct D band is observed in the Raman spectrum. The enhancement of the D band could be a result of defects created during the transfer process. c) The C1s core level XPS spectrum of the same sample reveals a substantial signal from other carbon functionalities and an increase in the sp^3 contribution. The asymmetry factor α on the graphitic peak is increased to 0.1. The transfer process induces a substantial amount of impurities and different functionalized carbon contaminants.

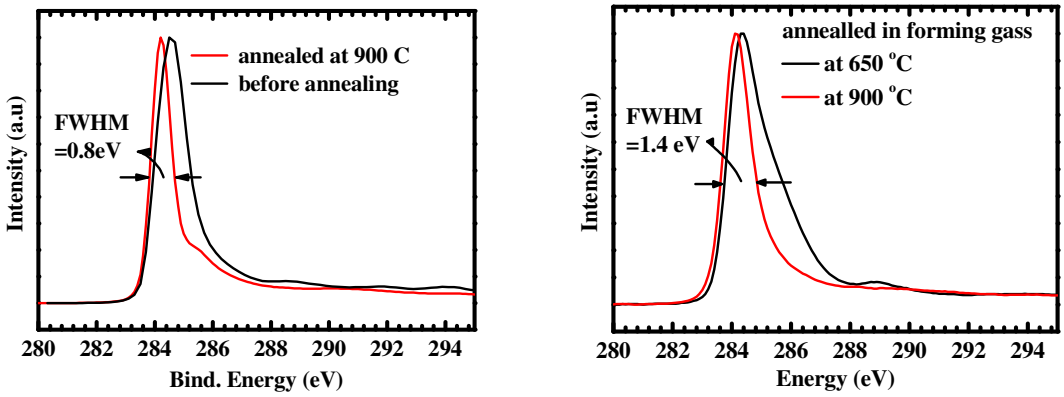

Figure 3 a) Few layer graphene transferred onto a SiO_2 substrate without the use of polymer support. The sample underwent annealing in forming gas for 10 hours at 900 ˚C. C1s core level XPS spectra of this sample are shown before and after the annealing step. The full width half maximum (FWHM) of the peak is reduced from 1.32 eV to 0.8 eV on annealing, indicating the removal of substantial amounts of contaminants. b) In the second case the same experiment was conducted using monolayer graphene which was transferred using a polymer support. The C1s peak of two different samples annealed in the same fashion at 650 ˚C and 900 ˚C are shown. In the best case (at 900 ˚C) the FWHM was 1.4 eV, which suggests that annealing does not remove polymer residues whereas this is feasible for low molecular weight adsorbents as shown in the first case.

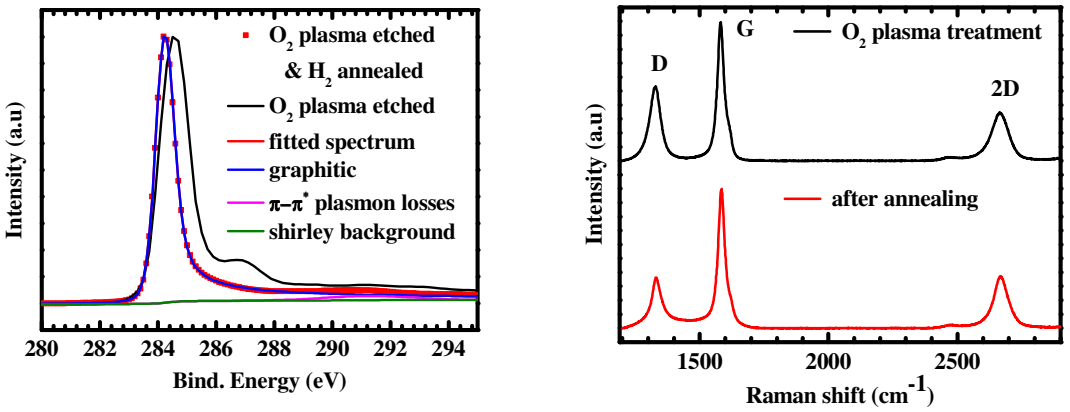

Figure 4 The use of plasma treatment combined with annealing as a cleaning step on graphene is shown. Few layer graphene, transferred as before on SiO_2 was treated with oxygen plasma for two minutes 4a) C1s XPS spectra of the sample before and after the annealing. The non-annealed sample (black colour) has a C1s peak shifted to higher energies, with a FWHM of 1.2 eV. An extra peak observed at 286.2 eV is due to epoxide formation on the graphitic net. After annealing the spectrum (dot spectrum) is sharper and still displays asymmetry on the higher binding energy side. The peak has shifted to lower binding energy and the epoxide peak has disappeared. The spectrum has a FWHM of 0.68 eV as extrapolated from the analytical fitting (shown), exactly the same as the instrumental resolution and shows a perfectly clean graphitic signal. There are no traces of any kind of carbon functional groups. The lower binding energy at 284.19 eV is due to better screening and extensive delocalization. This gives a strong indication that curing of defects on the graphitic net occurs. 4b) A Raman spectrum from the sample shows a reduced D band peak after annealing which further proves that curing of defects on the graphitic net occurs.

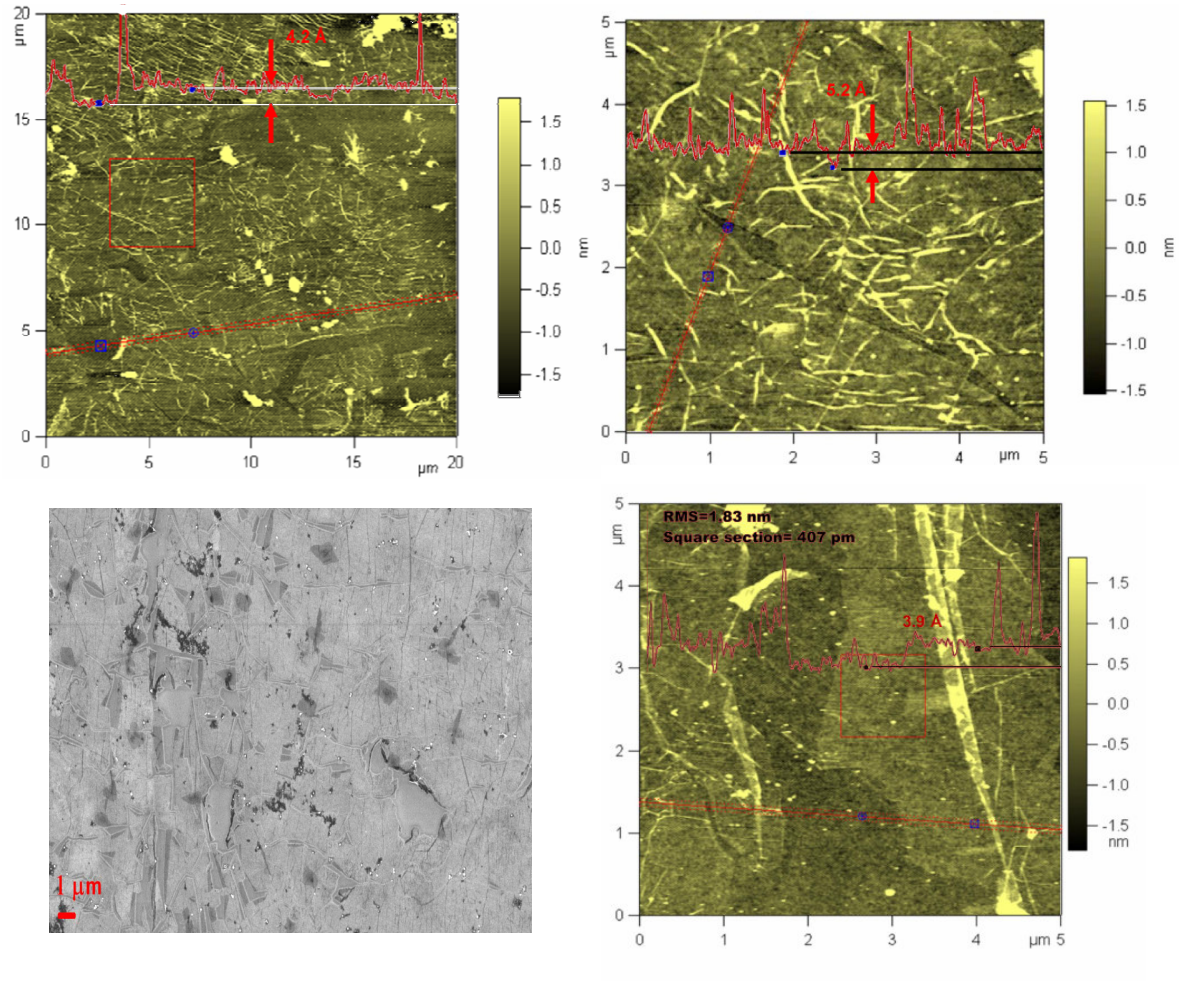

Figure 5 a) An AFM image of the plasma treated monolayer graphene is shown. The surface looks much cleaner and has a much smaller RMS roughness value of 2.9 nm compared to the untreated case. The step height from substrate to graphene is 0.42 nm, and is much smaller than that which has been published before for a monolayer graphene[24]. b) A higher magnification image shows distinguishable ripples and wrinkles on graphene which weren't observable before the treatment. c) Large area (~20 µm) SEM image of plasma treated graphene is presented which proves that this method is not highly destructive and can produce large area clean graphene films. d) AFM image of plasma treated grapheme shows a well preserved monolayer.

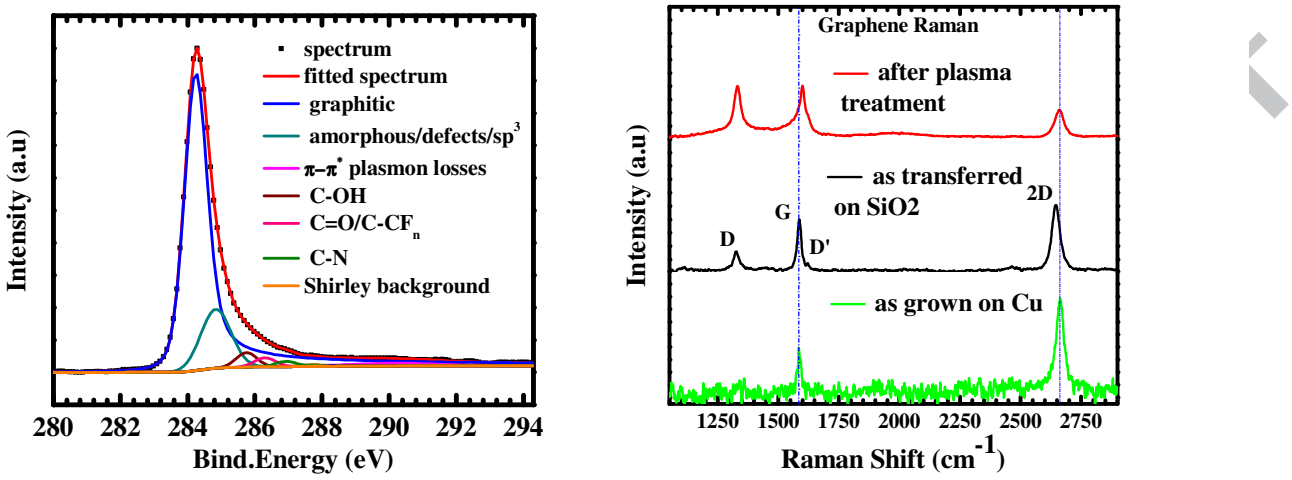

Figure 6 a) C1s core level spectrum of monolayer graphene treated with O_2/H_2 plasma in order to clean the surface. The spectrum comes with an asymmetry on the higher binding energy side of the peak which is located at 284.28 eV. The higher singularity asymmetry factor α of 0.08 and the slightly higher binding energy, compared to the spectrum of as grown graphene on Cu shown earlier, indicate a slightly defective graphitic net. Importantly, a second fitted peak at 284.8 eV, which accounts for amorphous carbon content and sp^3 defects, has been diminished proving that polymer residue contamination has been substantially reduced. The remaining peak at 284.8 eV related to sp^3 bonds in the graphitic net, may be explained by hydrogen incorporation during the hydrogen plasma step. b) Raman spectra of the three different steps are compared. The Raman spectrum after the cleaning treatment presents an enhanced D peak which is prominent of defective graphitic structure and is in agreement with the XPS observations.

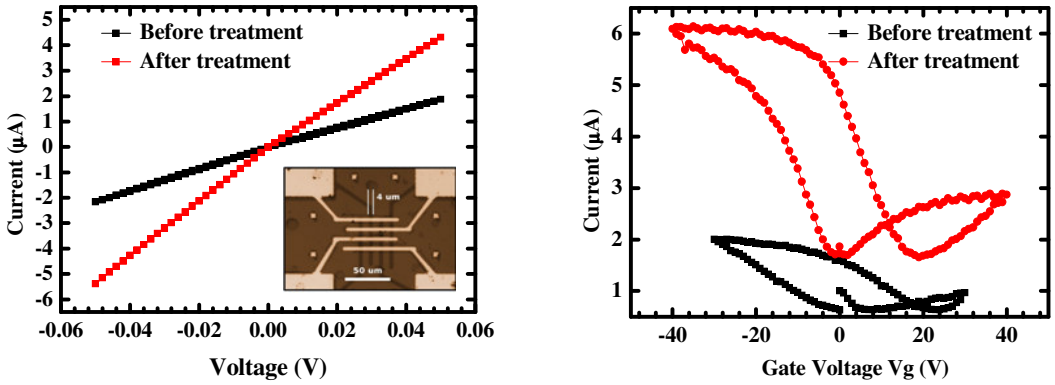

Figure 7 Structured and contacted graphene ribbons, were measured electrically before and after the plasma cleaning treatment. a) Graphene ribbons have shown linear source-drain current versus bias voltages (I_{ds}-V_{ds}) characteristics and conductivity increased approximately 1.5-6 times after the plasma treatment process. Inset: Structured graphene nanoribbons b) Typical ambipolar characteristics, with a higher hole conduction for graphene and hysteresis are observed in both cases. The electron and hole mobilities are increased from 11.2 and 31.9 cm^2/Vs respectively to 44.8 and 143.6 cm^2/Vs with plasma treatment.